

Multipass coherent processing on synthetic aperture sonar data

Stig A V Synnes, Hayden J Callow, Roy E Hansen, Torstein O Sæbø

Norwegian Defence Research Establishment (FFI), P O Box 25, NO-2027 Kjeller, Norway
{Stig-Asle.Synnes, Hayden-John.Callow, Roy-Edgar.Hansen, Torstein-Olsmo.Sabo}@ffi.no

We investigate whether coherent processing can be achieved on synthetic aperture sonar (SAS) data recorded on different passes over the same scene. A major challenge of multipass coherent processing on SAS images is the demand of accurate platform navigation and control. To overcome this we will correlate echoes from multiple passes in order to provide high fidelity navigation between the passes, supporting co-registration of SAS imagery with sub-resolution accuracy. This would provide a door-opener for multipass coherent processing on full resolution SAS images for products such as high resolution bathymetric mapping and coherent change detection. A dedicated experiment is run using the HISAS 1030 SAS on a HUGIN 1000-MR autonomous underwater vehicle (AUV). On the recorded data we demonstrate multipass coherent processing on ping pairs from different passes and obtain a normalized correlation coefficient exceeding 0.96 between time series of pings recorded one hour apart. We also present, to our knowledge, the first experimental assessment of the effect of cross-track separation on multipass coherent processing of SAS data. Finally we demonstrate that the navigation system can be updated with measurements from multipass coherent processing, and that such updates can reduce the navigation uncertainty between passes down to sub-wavelength scale.

1 Introduction

Multipass coherent processing on synthetic aperture sonar (SAS) images can provide full resolution phase maps applicable for coherent change detection, high accuracy bathymetric mapping and other coherent sonar products. To the best of our knowledge, multipass coherent processing on SAS data has not been published earlier. Multipass coherent processing is however well established in synthetic aperture radar (SAR) [1, 2]. For satellite borne SAR systems the technique has reached an extreme sophistication level [3]. Airborne systems have more challenges in vehicle guidance and motion control [4, 5]. Navigation and control is also a major challenge for multipass coherent processing on SAS systems.

Multipass coherent processing takes benefit of the similarity of two time series recorded at different times, but at roughly the same position. The similarity of the times series is reduced with the spatial separation between the sensor positions. Therefore, strong demands apply on the navigation and control systems in order to successfully achieve coherent processing. In this paper we focus on multipass coherent processing on individual ping pairs as a precursor to producing coregistered multipass SAS images. We demonstrate the estimation of multipass along-track and cross-track displacement for single pings using coherent processing on tracks crossing at small angles. We also estimate the maximum distance requirements for coherent multipass processing for both raw and beamformed element data. We note that ping-for-ping repeat pass processing has the potential to dramatically improve final SAS multipass processing by giving feedback to the vehicle navigation system in real-time and ensuring suitable sonar data collection.

In section 2 we give a brief description of the technique used for estimating time delay along with a performance measure. We also estimate theoretical upper limits on the maximum baseline allowed for multipass coherent processing. In section 3 we describe our experiment, the collection of data and our post processing algorithms. The results are presented in section 4 where we also estimate the experimental maximum baseline for multipass coherent processing. Finally, in section 5 we summarize the main findings, conclude and suggest future work.

2 Theory of coherent processing

Multipass coherent processing depends on matching the echoes (pings) from different lines, not only using their amplitude, but also their phase. The time-series from a single ping is the coherent sum of the echoes from each reflector within the sonar beamwidth. In order to achieve coherent processing over multiple passes, a near identical time series must be found / formed during the repeat pass. The similarity of the two time series will rapidly decrease with the separation of the sonar positions between two passes. However, we are encouraged by that interferometry on vertically displaced sensors on the same vehicle successfully produces bathymetry measurements [6]. Overlapping elements of a moving multielement array is also successfully correlated for estimating the array movement in SAS micronavigation [7].

A critical parameter for multipass coherent processing is therefore the degree of similarity between two time series. The ratio of the coherent energy to the total signal energy can be expressed as a measure of coherence [8]. In this section we first define the coherence measure mathematically

using two signal time series. Then we address some geometric effects which, if not compensated for, will reduce the coherence. Finally, we make a rough estimate of the maximum baseline between two tracks before decorrelating.

2.1 Coherence

We now define the coherence measure that will be used as a measure of similarity between two time series. Assume two receivers spatially displaced that record the scattered field time-series from a rough surface $s_1(t)$ and $s_2(t)$. The *mutual coherence function*, or the cross-correlation function, is defined as [9, pp 562-566]

$$\Gamma_{12}(\tau) = \langle s_1(t)s_2^*(t + \tau) \rangle, \quad (1)$$

where τ is a time-shift. We use the term *coherence* for the peak magnitude of the normalized cross correlation

$$\gamma = \arg \max_{\tau} \left| \frac{\Gamma_{12}(\tau)}{[\Gamma_{11}(0)\Gamma_{22}(0)]^{1/2}} \right|, \quad (2)$$

similar to the naming convention used in radar interferometry for coregistered images [2]. Note that in underwater acoustics [10] and signal processing [11] the term *coherence* is commonly used as the *spectral degree of coherence*, not to be confused with our use.

2.2 Geometric coherence effects

Deterministic geometric effects introduced when displacing one receiver relative to another can be (at least partially) compensated for. Compensating for such effects before multipass coherent processing will lead to a higher coherence and thereby a more accurate result.

We define a coordinate system at the sensor with the x-axis as the horizontal component along-track, the z-axis vertically down and the y-axis in the horizontal plane to form a right-handed coordinate system. Two other coordinate systems will also be used. The direction along a generally sloping sea bottom in our y-z plane is named *ground-range direction*, and the direction from the sensor to the sonar footprint on the bottom is named *slant-range direction*.

Some deterministic corrections comprise:

- Cross-track footprint shift: A shift of footprint between the two time series will reduce the overlapping signal and hence also the coherence. This can be adjusted for by shifting one of the time series.
- Along-track footprint shift: The along-track footprint of the beams can be steered to match each other.
- Ground-range mapping: A time series gives the distance from the transmitter-receiver to the sea floor in the slant-range direction. A different sensor position will result in a different slant-range direction and thus a compressed or elongated time series. However, if the bathymetry is known, this effect can be compensated by e.g. mapping to ground-range [12].

- Footprint (beam pattern) deformation: A different sensor position will give a different footprint shape in the horizontal plane. In principle, one can change the size of the footprint by changing the number of elements or by using a taper on the array. In practice, however, this is complicated and usually not done.

2.3 Spatial limitations

In the start of section 2 we indicated that whether multipass coherent processing will work on two time series depends on their coherence, and that this in turn depends on the spatial displacement between the sensors. In order to plan our experiment for multipass coherent processing, we will now try to predict the displacement bounds. Because of the complexity we do not aim for the exact solutions, but rather simple rules of thumb for displacements in the cardinal directions.

Along-track decorrelation

This derivation is the most straight-forward. The correlation properties are given by the autocorrelation of the aperture. For rectangular apertures the correlation function is thus a triangle

$$\Gamma_{12}(\tau) = \begin{cases} (1 - |\tau|/D) & , |\tau| < D \\ 0, & \text{otherwise,} \end{cases} \quad (3)$$

where D is the element length. The 0.5 correlation point, Δ_x , is thus $D/2$ for an effective receiver length D .

Cross-track out-of-plane decorrelation

This is most simply calculated by using the wavenumber shift [13].

$$\Gamma_{12}(\tau) \approx \frac{\sqrt{1 - z^2/\tau^2}(k_0 + k_b/2) + k_b/2 - k_0}{k_b}, \quad (4)$$

for center frequency, $k_0 = 2\pi/\lambda$ for wavelength λ , range, r , altitude z , and two-sided bandwidth $k_b = 2\pi/\lambda_b$. The 0.5 correlation point is given by

$$\Delta_z = \frac{2r_0\sqrt{2k_0k_b}}{2k_0 + k_b} \quad (5)$$

Cross-track in-plane decorrelation

This is more difficult to expand in closed form so we rather give a rough rule based on phase error. From [14] the phase error for a given range displacement, Δ_ϕ , is given as

$$\Delta_\phi = 2k_0\Delta_y(1 - \cos\theta), \quad (6)$$

putting in the 3 dB beamwidth angle θ_{3dB} gives the point where phase contributions become negative (which actually

occurs well before the 0.5 point in correlation value)

$$\Delta_y \approx \frac{\pi}{2k_0(1 - \cos \theta_{3\text{dB}})} \quad (7)$$

$$\approx \frac{\lambda}{4(\theta_{3\text{dB}}^2/2)} \quad (8)$$

Numeric results

For the experiments we use a dense sensor array of 32 elements, each 3.75 cm long (see Section 3.1). The operating frequencies are centered on 100 kHz. The signals are recorded individually at each sensor element, such that an effective array of any length from 1 through 32 elements can be obtained in the post processing. Here we choose to investigate the different power-of-two element lengths. A system of N combined elements will be called a system of *superelement* N .

Inserting the sonar specifications in Equations (3), (5) and (8), we obtain Table 1. Note that this should be read as an indication of the upper limit of the displacement. Equations (3), (5) and (8) are approximate and describe the ideal case with both sensors mapping the same footprint from the same direction. This will not be the case in real measurements, and any uncompensated geometric effects could lead to a significant reduction of the coherence.

N	$\theta_{3\text{dB}}$	Δ_x	Δ_y	Δ_z
32	0.63	0.60	192	75
16	1.2	0.30	48	75
8	2.5	0.15	12	75
4	5.0	0.07	3.0	75
2	10.1	0.04	0.75	75
1	20.3	0.02	0.19	75

Table 1: Two-sided 3dB beamwidth (in degrees) and indication of the upper limit of displacement (in meters) allowing for multipass coherent processing versus superelement size, specified as number of elements of length 3.75 cm.

3 Experiment

The main goal with the experiment is to provide data for multipass coherent processing. This would generally require co-registration of the navigation tracks with sub-wavelength accuracy in both the along-track and slant-range directions.

We know from SAS microneavigation (DPCA) that the highest accuracy in the along-track correlation is achieved by operating on single elements [7]. Because we have a dense array, the predicted decorrelation along the x-axis is overcome by correlating combinations of different elements from both tracks until a match is found. In the range-direction, however, the second track must be within a small distance from the first track. The predictions from Table 1 indicates that only around 0.2 m deviation is accepted when using a single element, but that this limit rapidly increases up to 48 m for

superelement 16. We also recall that only speckle decorrelation was estimated, and other effects might reduce the limits significantly.

The navigation and control systems of autonomous underwater vehicles (AUV) are not yet accurate enough to repeat a track within in 0.2 m accuracy. In order to assure that we have at least some data with the required position overlap, we chose to record data from tracks crossing at small angles. Two sets of data were record with intersection angles planned at 5.0 degrees and 0.5 degrees. In the rest of this chapter we describe our platform, the tracks and the data processing.

3.1 Platform and sensor

The sonar measurements were conducted with the HISAS 1030 synthetic aperture sonar on a HUGIN 1000-MR autonomous underwater vehicle, as illustrated in Figure 1.

The HISAS 1030 has a single transmitter and 32 receiver elements arranged in a dense array along-track. Each element is 3.75 cm long. During the experiment the system was operated with a 30 kHz bandwidth around 100 kHz, corresponding to a wavelength of around 1.5 cm. The received time series were recorded individually for each sensor, allowing for post processed beamforming. In particular we are able to combine elements to different superelement sizes and beamwidths as outlined in Table 1.

During the experiment the navigation was based on an inertial navigation system (INS) supported by a Doppler velocity logger. Navigation data were subsequently post-processed with the NavLab navigation system [15].



Figure 1: HISAS on HUGIN 1000 MR.

3.2 Track planning

The AUV was programmed to first run one straight line, and then return after an hour and repeat the start of the line. Because of the uncertainty of the AUV position during the second pass relative to the first one, the line was planned to be 500 m long and to cross with an intersection at 5 degrees around a heading of 160 degrees. In addition, two other

lines were recorded 10 minutes apart, 400 m long and with a planned intersection angle of 0.5 degrees around a heading of -20 degrees. Thus we would obtain sonar measurements both from the same position at the crossing of the lines, but also at different separation distances in the cross-track direction, allowing for investigation of the decorrelation distance. The tracks of both the 5 degrees and 0.5 degrees crossings are illustrated in Figures 2 and 3 on top of the sidescan images recorded during their first passes.

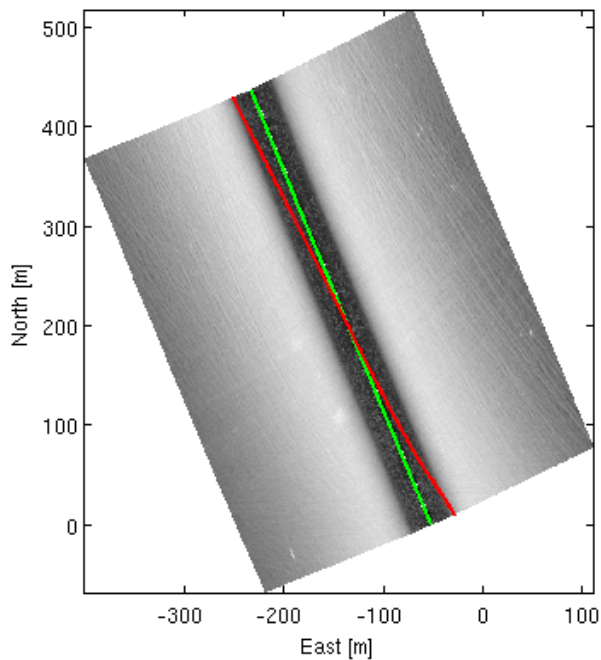


Figure 2: Sidescan image of pings 60–960 (from top to bottom) of the first track of the two passes crossing at 5.0 degrees. The trajectory of the navigation system of the first track is plotted in green and the second track in red.

3.3 Method

As outlined in section 2, the processing is closely related to that of interferometry and SAS microneavigation. For a given pair of (super)elements we estimate the time delay, and the maximum coherence which is used to give the quality of the estimate.

A main difference is the initial uncertainty of the sensor positions, demanding a search over different pings and elements for correlating pairs. Before correlating the time series, the multielement arrays of the second track are steered to look in the same direction as that of the first track. We have not yet converted the time series to ground-range, and thus with an AUV height of 20 m above the seafloor we select a data patch centered at 100 m distance in order to reduce the deformation effects between the two time series. Small patches are also less affected by stretching effects, but random noise is reduced with longer patches. We compro-

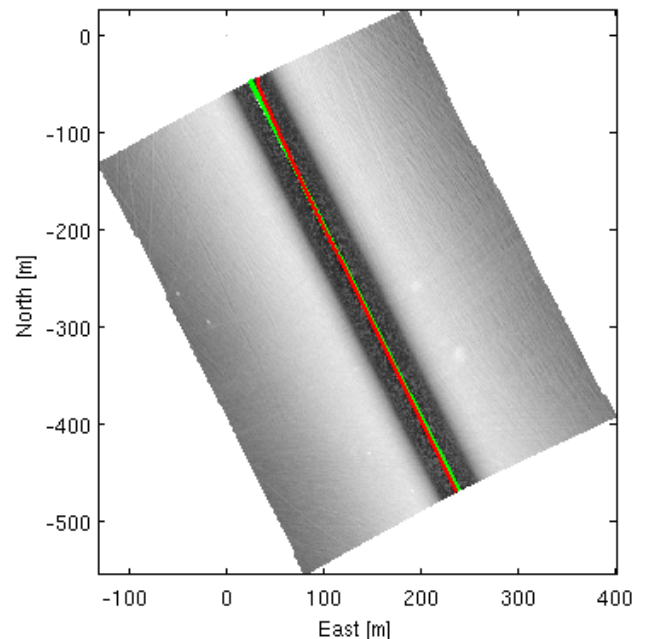


Figure 3: Sidescan image of pings 100–1000 (from bottom to top) of the first track of the two passes crossing at 0.5 degrees. The trajectory of the navigation system of the first track is plotted in green and the second track in red.

mise with a patch length of 4 m. After the first correlation, the correlation is recomputed with the footprint shifted in range according to the first estimate. The along-track AUV displacement per ping is approximately 0.53 m.

4 Results and analysis

In this section we first present the obtained displacement estimate per ping along with the corresponding coherence. We then rearrange these results to express the coherence versus estimated displacement, thereby indicating the cross-track in-plane decorrelation.

4.1 Results per ping

Through our data processing we identified coherent ping pairs and element pairs from the two tracks. We also obtained the time delay and coherence for the matching pairs. The time delay was converted to slant-range track separation using a sound velocity of 1500 m/s. The resulting track separation versus ping number is illustrated in Figure 4 for the 5 degrees crossing and in Figure 5 for the 0.5 degrees crossing.

The 5 degrees crossing is most easily analyzed. Here we estimate a linearly decreasing distance between the tracks from around 1.5 to -1.5 m, consistent with the crossing of the tracks as illustrated in Figure 2. These estimates are plot-

ted for superelement 16. Consistent estimates correspond to coherence values of roughly 0.5 or higher.

While the 5 degrees crossing in Figure 4 is illustrated through 120 pings, the 0.5 degrees crossing of Figure 5 keeps a small separation for longer time and the illustration includes close to 1000 pings. From the estimated distance between the tracks, it is apparent that the AUV track were not entirely straight over all these pings and we have far more pings of positive distance than with negative distance.

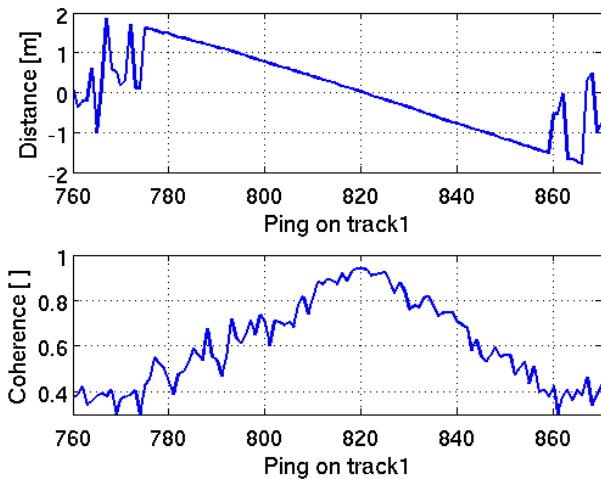


Figure 4: Estimated coherence and track separation versus ping number for the 5 degrees crossing with superelement 16.

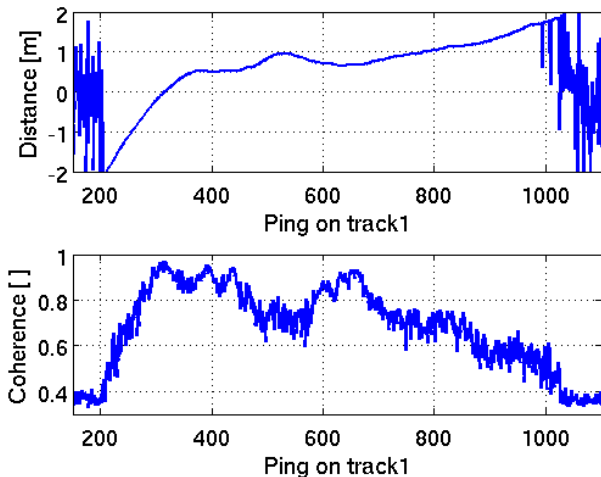


Figure 5: Estimated coherence and track separation versus ping number for the 0.5 degrees crossing with superelement 16.

4.2 Navigation

The estimated position of zero cross-track separation is for the 5 degrees crossing near ping 820 of track 1, and for the

0.5 degrees crossing near ping 300 of track 1. The correlating ping of the second track for each crossing must thus have been recorded at the same position. The AUV sailed for one hour between the two tracks of the 5 degrees crossings, and when we compare the position estimates of the navigation system at those ping pairs, the navigation system reports a predicted displacement in the cross-track direction of 1.6 m with an uncertainty of several meters. Between the 0.5 degrees crossing the AUV sailed for approximately 10 minutes. Here the navigation system reported a cross-track separation of 0.88 m with accuracy of around a meter. Thus the navigation system appears to be operating within its typical uncertainty bound. We note that by including information from the multipass coherent processing the uncertainty of the relative navigation estimate can be reduced to sub-wavelength or millimeter accuracy.

4.3 Coherence versus distance

In this section we rearrange the results of section 4.1 to express the coherence versus the estimated displacement. This is done for all the tested superelements and each ping. The results are presented in Figure 6 for the 5 degrees crossing and in Figure 8 for the 0.5 degrees crossing.

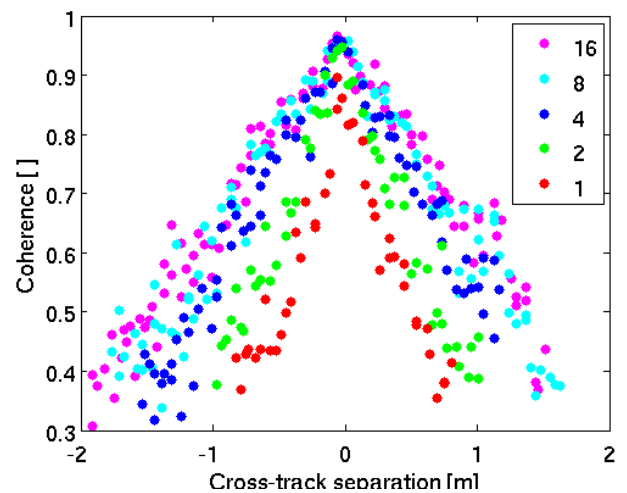


Figure 6: 5 degrees crossing: Coherence versus cross-track separation for the best ping- and superelement pairs of pass 1 and 2. The coherence is presented for superelement sizes of 1 through 16 elements of 3.75 cm length.

For the 5 degrees crossing, we observe a triangular shape of the coherence as function of the cross-track separation. This is repeated for all superelements. The accepted cross-track separation is increasing with the superelement number, but does in general not follow the predicted distances of Table 1. The predictions dictated that the distance should increase with the number of elements squared, while the actual increase follows roughly the logarithm of the number of elements.

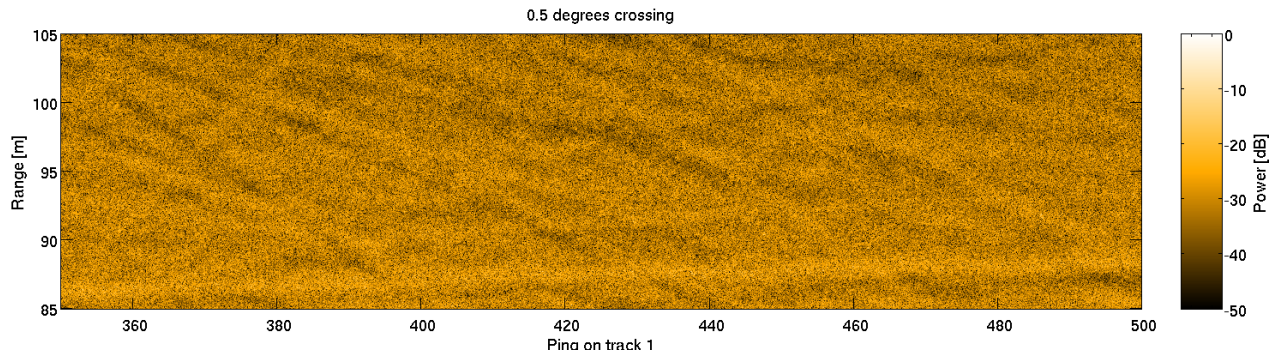


Figure 7: SAS image of scene.

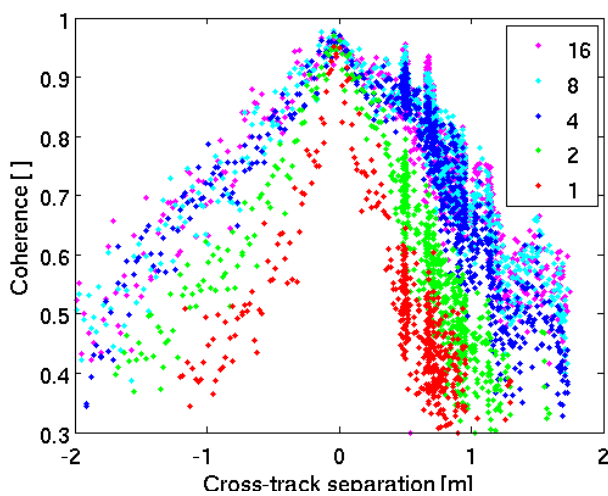


Figure 8: 0.5 degrees crossing: Coherence versus cross-track separation for the best ping- and superelement pairs of pass 1 and 2. The coherence is presented for superelement sizes of 1 through 16 elements of 3.75 cm length.

The results for the 0.5 degrees crossing confirm the general findings from the 5 degrees crossing. However, with many more pings within the critical baseline (in particular for positive cross-track separation) we have much more data for this crossing. Those reveal a larger span of the coherence values, and in particular we note two deviations in the distribution around cross-track separation 0.5 m and 0.7 m. Here the coherence for superelements 4 through 16 are increased, while the coherence for superelement 1 is decreased. The reasons for this is yet to be understood. Among other candidates, the geometry of the tracks and possible objects on the scene could have such an effect. Conferring Figure 5 we conclude that most of the pings around 0.5 m and 0.7 m cross-track separation must come from around pings 390 to 480 and pings 600-670 respectively. In Figure 7 we show the SAS image of the first of those ping intervals. We observe that the seafloor consists of sand-like bottom with trawl-tracks but with no obvious strong or large object.

5 Conclusion

We have successfully planned a measurement campaign for demonstrating coherent multipass processing on a SAS system and demonstrated high coherence on the collected data set. This was done in despite of the challenges of navigation accuracy related to multipass coherent processing. We have collected and presented the, to our knowledge, first experimental assessment of the effect of cross-track separation on multipass coherent processing of SAS data. Our results will be important for the planning and execution of further experiments, and in particular for collecting data for coherent processing of SAS image pairs. However, as the results did not match the theoretical predictions, this will also be a topic for further work. Finally we demonstrated that navigation systems can be updated by measurements from multipass coherent processing, and that such updates can reduce the navigation uncertainty between tracks to millimeter scale.

We believe that the demonstrated ping-by-ping coherent processing will support generation of coherent SAS image pairs. Coherent SAS image pairs opens for coherent change detection, high accuracy bathymetric mapping and other coherent sonar products, which should be a goal of future work.

Acknowledgment

Thanks to Einar Berglund, FFI, for fruitful discussions during mission planning.

References

- [1] P. A. Rosen, S. Hensley, I. R. Joughin, F. K. Li, S. N. Madsen, E. Rodriguez, and R. M. Goldstein. Synthetic aperture radar interferometry. *Proceedings of the IEEE*, 88(3):333–382, 2000.
- [2] R. F Hanssen. *Radar Interferometry: Data Interpretation and Error Analysis*. Kluwer Academic Publishers, 2001.
- [3] G. Krieger, I. Hajnsek, K. P. Papathanassiou, M. Younis, and A. Moreira. Interferometric synthetic aperture radar (sar) missions employing formation flying. *Proceedings of the IEEE*, 98(5):816–843, May 2010.
- [4] A. L. Gray and P. J. Farris-Manning. Repeat-pass interferometry with airborne synthetic aperture radar. *IEEE Trans. Geosci. Remote Sensing.*, 31(1):180–191, January 1993.
- [5] S. Perna, C. Wimmer, J. Moreira, and G. Fornaro. X-band airborne differential interferometry: Results of the OrbiSAR campaign over the perugia area. *IEEE Trans. Geosci. Remote Sensing.*, 46(2):489–503, February 2008.
- [6] T. O. Sæbø, B. Langli, H. J. Callow, E. O. Hammerstad, and R. E. Hansen. Bathymetric capabilities of the HISAS interferometric synthetic aperture sonar. In *Proceedings of OCEANS 2007 MTS/IEEE*, Vancouver, Canada, October 2007.
- [7] A. Bellettini and M. A. Pinto. Theoretical accuracy of synthetic aperture sonar micronavigation using a displaced phase-center antenna. *IEEE J. Oceanic Eng.*, 27(4):780–789, 2002.
- [8] D. C. Ghiglia and M. D. Pritt. *Two-Dimensional Phase Unwrapping: Theory, Algorithms, and Software*. John Wiley & Sons, INC, New York, NY, USA, 1998.
- [9] M. Born and E. Wolf. *Principles of Optics*. Pergamon press, 7th expanded edition, 1999.
- [10] G. C. Carter. Coherence and time delay estimation. *Proceedings of the IEEE*, 75(2):236–255, February 1987.
- [11] R. Shiavi. *Introduction to Applied Statistical Signal Analysis*. Academic Press, 1999.
- [12] T. O. Sæbø, R. E. Hansen, and A. Hanssen. Relative height estimation by cross-correlating ground-range synthetic aperture sonar images. *IEEE J. Oceanic Eng.*, 32(4):971–982, October 2007.
- [13] F. Gatelli, A. M. Guarnieri, F. Parizzi, P. Pasquali, C. Prati, and F. Rocca. The wavenumber shift in SAR interferometry. *IEEE Trans. Geosci. Remote Sensing.*, 32(4):855–865, July 1994.
- [14] H. J. Callow, M. P. Hayes, and P. T. Gough. Motion-compensation improvement for widebeam, multiple-receiver SAS systems. *IEEE Journal of Oceanic Engineering*, 34:262–268, 2009.
- [15] K. Gade. Navlab, a generic simulation and post-processing tool for navigation. *European journal of navigation*, 2 (4):51–59, 2004.